

Article

Tunable Non-Enzymatic Glucose Electrochemical Sensing Based on the Ni/Co Bimetallic MOFs

Qi Wang^{1,2}, Qi Jia^{1,2}, Peng Hu^{2,*}  and Liudi Ji^{2,*} 

¹ School of Pharmacy, Hubei University of Science and Technology, Xianning 437100, China; hy33601@163.com (Q.W.); jq_958@163.com (Q.J.)

² Hubei Key Laboratory of Radiation Chemistry and Functional Materials, Hubei University of Science and Technology, Xianning 437100, China

* Correspondence: hupeng@hust.edu.cn (P.H.); jiliudi@126.com (L.J.)

Abstract: Constructing high-performance glucose sensors is of great significance for the prevention and diagnosis of diabetes, and the key is to develop new sensitive materials. In this paper, a series of Ni₂Co₁-L MOFs (L = H₂BPDC: 4,4'-biphenyldicarboxylic acid; H₂NDC: 2,6-naphthalenedicarboxylic acid; H₂BDC: 1,4-benzenedicarboxylic acid) were synthesized by a room temperature stirring method. The effects of metal centers and ligands on the structure, compositions, electrochemical properties of the obtained Ni₂Co₁-L MOFs were characterized, indicating the successful preparation of layered MOFs with different sizes, stacking degrees, electrochemical active areas, numbers of exposed active sites, and glucose catalytic activity. Among them, Ni₂Co₁-BDC exhibits a relatively thin and homogeneous plate-like morphology, and the Ni₂Co₁-BDC modified glassy carbon electrode (Ni₂Co₁-BDC/GCE) has the highest electrochemical performance. Furthermore, the mechanism of the enhanced glucose oxidation signal was investigated. It was shown that glucose has a higher electron transfer capacity and a larger apparent catalytic rate constant on the Ni₂Co₁-BDC/GCE surface. Therefore, tunable non-enzymatic glucose electrochemical sensing was carried out by regulating the metal centers and ligands. As a result, a high-sensitivity enzyme-free glucose sensing platform was successfully constructed based on the Ni₂Co₁-BDC/GCE, which has a wide linear range of 0.5–2899.5 μM, a low detection limit of 0.29 μM (S/N = 3), and a high sensitivity of 3925.3 μA mM⁻¹ cm⁻². Much more importantly, it was also successfully applied to the determination of glucose in human serum with satisfactory results, demonstrating its potential for glucose detection in real samples.



Citation: Wang, Q.; Jia, Q.; Hu, P.; Ji, L. Tunable Non-Enzymatic Glucose Electrochemical Sensing Based on the Ni/Co Bimetallic MOFs. *Molecules* **2023**, *28*, 5649. <https://doi.org/10.3390/molecules28155649>

Academic Editor: Liming Fan

Received: 30 June 2023

Revised: 19 July 2023

Accepted: 24 July 2023

Published: 26 July 2023



Copyright: © 2023 by the authors. Licensee MDPI, Basel, Switzerland. This article is an open access article distributed under the terms and conditions of the Creative Commons Attribution (CC BY) license (<https://creativecommons.org/licenses/by/4.0/>).

Keywords: 2D MOFs; metal centers; ligands; tunable electrochemistry; glucose sensing

1. Introduction

Glucose is one of the essential nutrients for human metabolism, but diabetes can be triggered when blood sugar levels are higher than normal. As we all know, diabetes is one of the most common chronic diseases in our daily life and is a serious threat to people's health [1,2]. Therefore, there is a significant medical value and commercial prospect to developing a stable and accurate glucose sensor for rapid real-time monitoring of blood glucose levels. To develop cheap and practical sensors, researchers have tried many new materials, according to the different catalytic mechanisms of these materials. The detection methods can be divided into colorimetry, fluorescence spectrometry, electrochemical method, etc. [3–5]. In contrast, the electrochemical method has the advantages of being convenient, rapid, sensitive, and economical and is the most widely used method for the determination of glucose content [6,7]. At present, most of the small blood glucose monitors on the market are enzyme-based blood glucose sensors, which have the advantages of high sensitivity and selectivity. However, there are also some insurmountable defects, such as the high cost and harsh survival conditions of biomolecular enzymes, and they are also susceptible to the influence of the external environment, such as temperature and pH. Therefore, it is essential to prepare enzyme-free glucose sensors that have a simple in

process, are less influenced by external factors, and are easily stored. Recently, enzyme-free glucose sensors have been developed by researchers using precious metals [8–10], inorganic carbon materials [11,12], transition metals and their oxides [13–15], nitrides and phosphides [16,17]. However, many of them still suffer from low catalytic activity, low sensitivity, and surface poisoning. Therefore, it is crucial to develop new high-performance, highly sensitive, and selective nanomaterials to construct efficient glucose sensors.

Metal-organic frameworks (MOFs) are a kind of porous coordination polymer with periodic network structures that are composed of metal ions or metal clusters and organic ligands [18]. With the advantages of an abundant ligand source and metal source, orderly and adjustable porous structure, large specific surface area, good thermal stability, they have been widely used in gas storage and separation [19,20], energy storage and conversion [21,22], molecular detection and contaminant identification [23,24], etc. Moreover, MOFs are rich in unsaturated metal active sites, which gives them good potential for electrochemical catalysis and sensing [25,26]. Compared with conventional bulk MOFs, 2D MOFs have nanoscale thickness and more uniform dimensions, which are favorable for mass transfer and fast electron transfer. Furthermore, the lamellar structure can expose more accessible active sites, which results in better electrochemical properties [27–29]. In addition, it was shown that there is a synergistic effect between the metals of bimetallic MOFs, which can effectively improve the catalytic activity [30,31]. Therefore, the construction of a highly sensitive and selective glucose electrochemical monitoring platform with 2D bimetallic MOFs has a very promising future. Moreover, it is innovative to carry out the research on how the metal centers and ligands affect glucose sensing performance.

Nickel and cobalt are widely used in the field of glucose catalysis because of their abundant source, low price, and high electrocatalytic activity [32,33]. So, in this study, Ni and Co were selected as metal centers, dicarboxylic acids of different chain lengths (H_2BPDC , H_2NDC , H_2BDC) were chosen as organic ligands, and a series of Ni_2Co_1-L MOFs (Ni_2Co_1-BDC , Ni_2Co_1-NDC , Ni_2Co_1-BPDC) were prepared by the room temperature stirring method. The patterns of influence of metal center types, ratios, ligands on their electrochemical properties were investigated. The Ni_2Co_1-BDC modified glassy carbon electrode (Ni_2Co_1-BDC/GCE) has a relatively large electrochemically active area and exposes more accessible catalytically active sites with high glucose catalytic activity. The mechanism of glucose oxidation signal enhancement was further investigated. The results demonstrated that glucose has a high electron transfer capacity and a large apparent catalytic rate constant on the Ni_2Co_1-BDC/GCE surface. Ultimately, a highly sensitive enzyme-free glucose sensing platform was successfully constructed based on the Ni_2Co_1-BDC/GCE . It was used for an actual human serum assay, and the results were consistent with hospital assays, indicating its good application prospects.

2. Results and Discussion

2.1. Characterization of Ni_2Co_1-L MOFs

Additionally, the crystallinity and phase purity of the synthesized Ni_2Co_1-L MOFs were examined using XRD, and the results are shown in Figure 1A–C. With the exception of some deviations in the relative intensities, their XRD patterns were in good agreement with the simulated patterns, which indicated the formation of high purity [34–36]. By comparing the FTIR spectra in Figure 1D, it can be seen that some absorption bands are the same in Ni_2Co_1-BPDC , Ni_2Co_1-NDC , and Ni_2Co_1-BDC MOFs. These indicated that they share common organic functional groups. The bending vibrations of the aromatic ring are about 678, 742, and 803 cm^{-1} [37]. Furthermore, they all have two characteristic peaks around 1375 and 1583 cm^{-1} , which correspond to the asymmetric stretching vibration peak (*as*) and the symmetric (*ss*) stretching vibration peak of the carboxyl group. The presence of a broad absorption band at 3394 cm^{-1} and the characteristic peak at 3598 cm^{-1} are due to the -OH vibration of water molecules present in the material structures [38]. All of these confirmed the successful introduction of ligands into the synthesized MOFs. In particular, the XRD diffraction peaks and FTIR patterns of Ni_2Co_1-BDC were basically in agreement with those

of the monometallic Ni-BDC and Co-BDC (Figure S1A,B in Supporting Information), which indicated that the introduction of Ni, Co bimetals did not affect the crystalline structure of MOFs. TGA analysis was applied to investigate the thermal stability of $\text{Ni}_2\text{Co}_1\text{-L}$ MOFs in the range of 25–700 °C. The results are shown in Figure S1C. The main weight loss of $\text{Ni}_2\text{Co}_1\text{-L}$ MOFs in the range of 25–170 °C was attributed to water and residual solvents adsorbed within the pores [39]. The second weight loss around 200–280 °C was attributed to coordinated water molecules, and the weight loss around 400 °C was assignable to decomposition of the carboxylate ligand [40]. As a comparison, $\text{Ni}_2\text{Co}_1\text{-BDC}$ had less percent weight loss, which resulted in better stability.

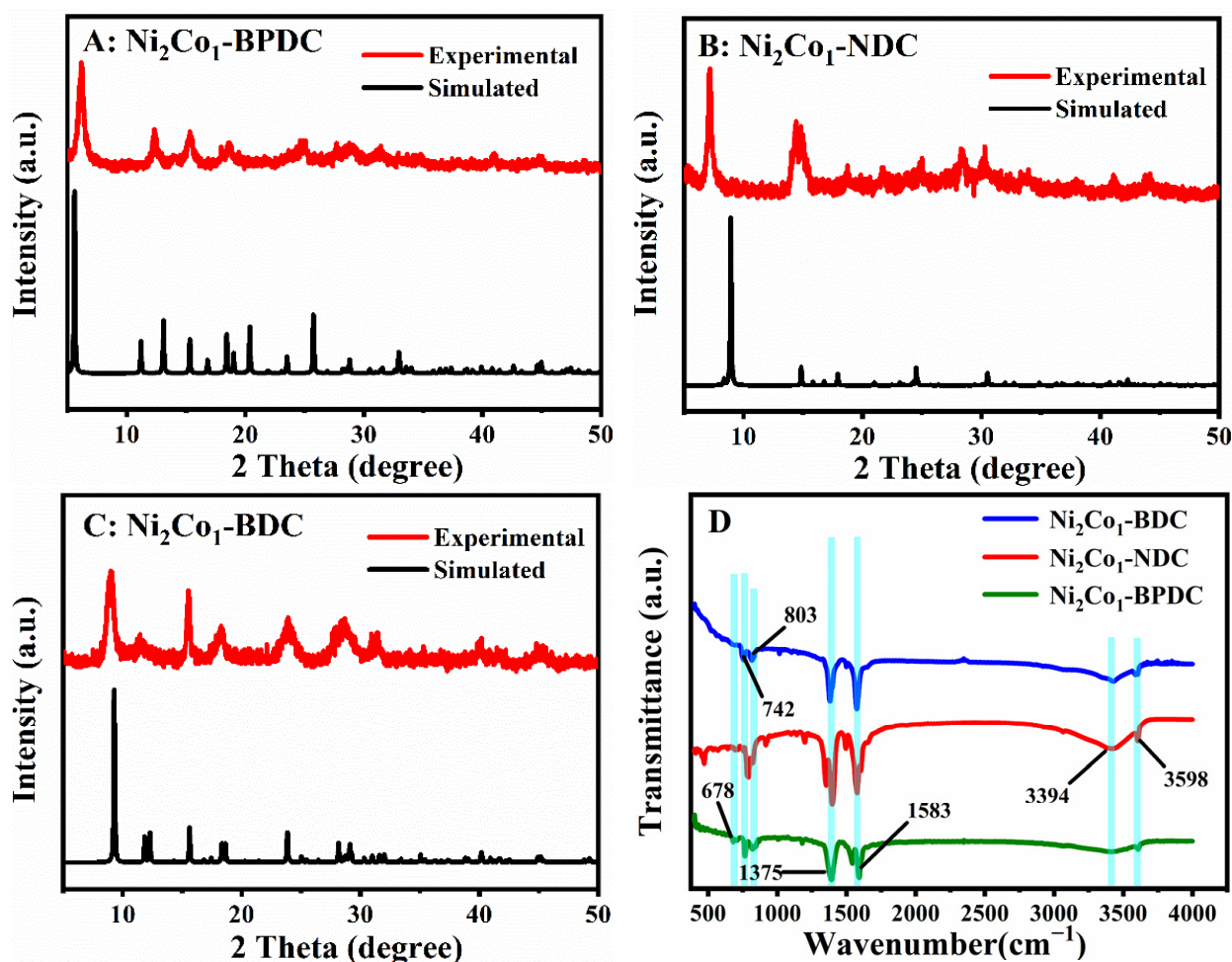


Figure 1. (A–C) XRD patterns of $\text{Ni}_2\text{Co}_1\text{-L}$ MOFs. (D) FTIR spectra of $\text{Ni}_2\text{Co}_1\text{-L}$ MOFs.

Then, the morphological characteristics of the synthetic materials were investigated using the SEM technique, and the corresponding images are shown in Figure 2. It can be seen from Figure 2A that the $\text{Ni}_2\text{Co}_1\text{-BPDC}$ is a layered stacking structure consisting of nanosheets with smaller sizes. $\text{Ni}_2\text{Co}_1\text{-NDC}$ (Figure 2B) is a bulky structure. On the contrary, $\text{Ni}_2\text{Co}_1\text{-BDC}$ (Figure 2C) is a relatively thin and homogeneous plate-like morphology, which possesses a 2D structure at the micron size. Then, the elemental distribution and content were characterized by EDS. From Figure 2D and Table S1 (Supporting Information), it can be seen that C, O, Ni, and Co are uniformly distributed on the surface of $\text{Ni}_2\text{Co}_1\text{-BDC}$.

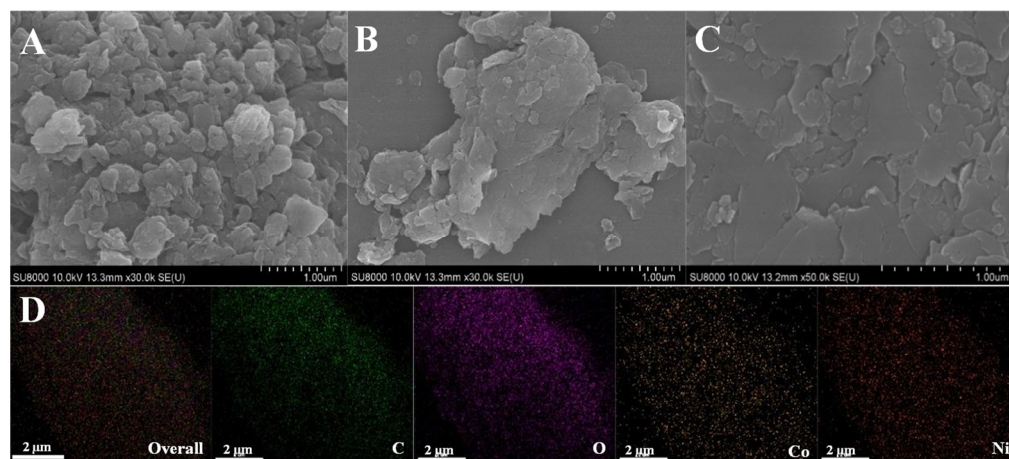


Figure 2. SEM images of Ni₂Co₁-BPDC (A), Ni₂Co₁-NDC (B), Ni₂Co₁-BDC (C). (D) EDS mapping images of Ni₂Co₁-BDC.

2.2. Electrochemical Performance of Ni₂Co₁-L MOFs

First of all, the electrochemical active areas of different Ni₂Co₁-L MOF nanosheets were compared by calculating the electric double-layer capacitance (C_{dl}) based on the CV tests in a non-Faradaic region (e.g., from 0.10 to 0.20 V) [41]. The results are shown in Figure 3A–C. According to the slope of the linear relationship between the capacitive currents difference ($\Delta j = j_{anodic} - j_{cathodic}$) at 0.15 V and the scan rates (Figure 3D), the C_{dl} of the Ni₂Co₁-BPDC/GCE, Ni₂Co₁-NDC/GCE, and Ni₂Co₁-BDC/GCE was obtained to be 3.20, 4.65, and 5.35 mF cm⁻², respectively. It is known that the C_{dl} is proportional to the electrochemically active area. The Ni₂Co₁-BDC/GCE had the largest active area, which may be derived from its 2D lamellar morphology.

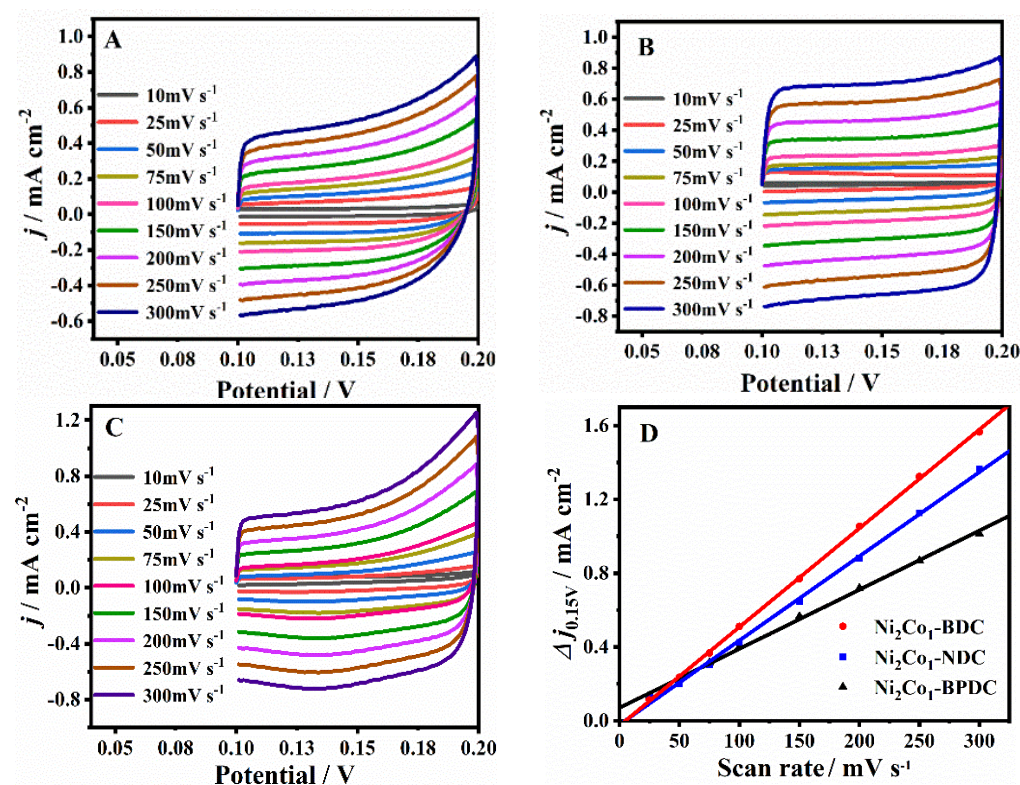


Figure 3. CV curves of the Ni₂Co₁-BPDC/GCE (A), Ni₂Co₁-NDC/GCE (B), Ni₂Co₁-BDC/GCE (C) at different scan rates in 1 M KOH; (D) linear plot of current density versus scan rates at 0.15 V.

It is well known that one of the key factors affecting the catalytic performance of electrode material is the number of active sites, which can be measured in the electrochemically active region. Here, the electrocatalytic activity of Ni₂Co₁-L MOFs was compared by recording the CV curves in 0.1 M NaOH at a scan rate of 100 mV/s, and the results are shown in Figure 4A. It is noteworthy that the GCE and Ni₂Co₁-BPDC/GCE show no obvious redox peak, suggesting poor electrochemical activity. The Ni₂Co₁-NDC/GCE shows a pair of asymmetric redox peaks at around 0.42 and 0.24 V, and in the CV curves of the Ni₂Co₁-BDC/GCE more obvious redox peaks appear at around 0.46 and 0.34 V. These redox peaks most likely resulted from the redox of their metal centers Ni²⁺ and Co²⁺. Additionally, the Ni₂Co₁-BDC/GCE has a higher peak current, suggesting the largest number of exposed active sites. Then, glucose was chosen as the target molecule and the catalytic activity of these materials on glucose was investigated. Figure 4B shows the CV curves of different GCEs after the addition of 0.1 mM glucose. No obvious redox peaks were observed on the surfaces of the GCE and Ni₂Co₁-BPDC/GCE. For the Ni₂Co₁-NDC/GCE and Ni₂Co₁-BDC/GCE, both of them show an oxidation peak with enhanced signal compared with Figure 4A without glucose. It was found that the Ni₂Co₁-BDC/GCE had the most obvious phenomenon, which indicated that it had the strongest catalytic activity for the oxidation of glucose. This can be attributed to the unique disk-like structure of Ni₂Co₁-BDC, as it exposes more active sites easily, like the results we mentioned above. The electrode reaction mechanism of the redox process can be expressed by the following equation [42]:

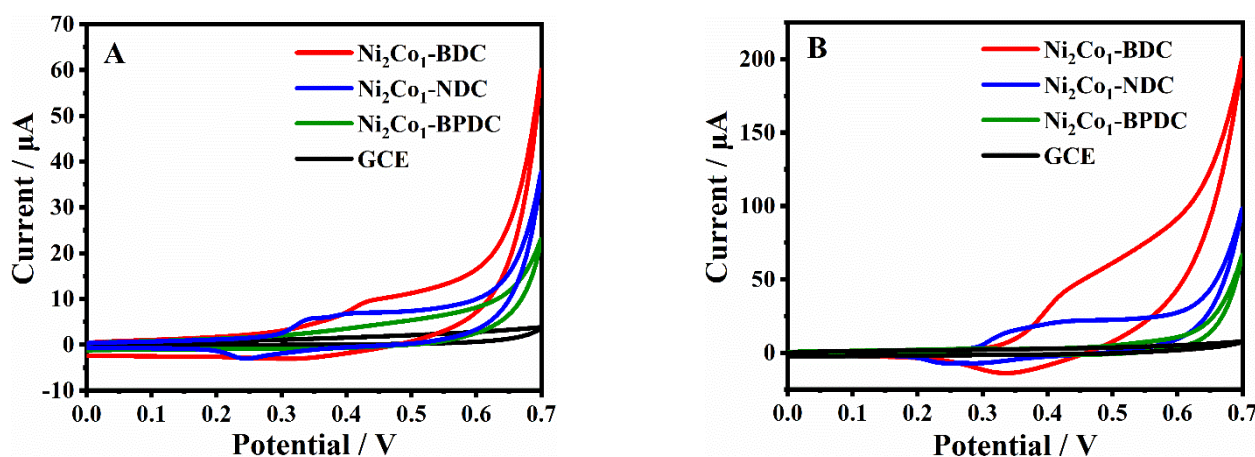
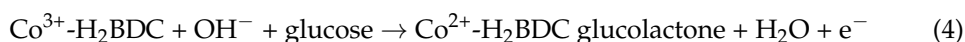
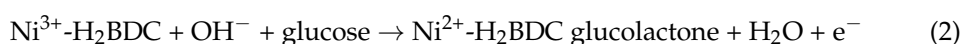
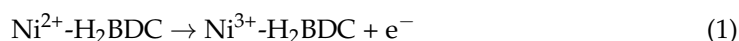


Figure 4. (A) CV curves for GCEs at 100 mV/s in 0.1 M NaOH. (B) CV curves for GCEs at 100 mV/s in 0.1 M NaOH with 0.1 mM glucose.

2.3. Electrochemical Oxidation of Glucose on Ni₂Co₁-L/GCEs

To further demonstrate the electrocatalytic activity of the series Ni₂Co₁-L MOFs for glucose oxidation, the *i-t* response of glucose on the surface of different GCEs was investigated. As shown in Figure 5A, *i-t* curves were recorded at 0.5 V for different GCEs after successive addition of 0.1 mM glucose in 0.1 M NaOH solution. No current step signal of glucose was observed on the bare GCE, indicating poor electrochemical activity. The current step signal of the Ni₂Co₁-BPDC/GCE had a slight increase, but it is difficult to

maintain a smooth state. In contrast, a remarkable increase was noticed in both the Ni₂Co₁-NDC/GCE and Ni₂Co₁-BDC/GCE, and the current step signal of the Ni₂Co₁-BDC/GCE had the largest value.

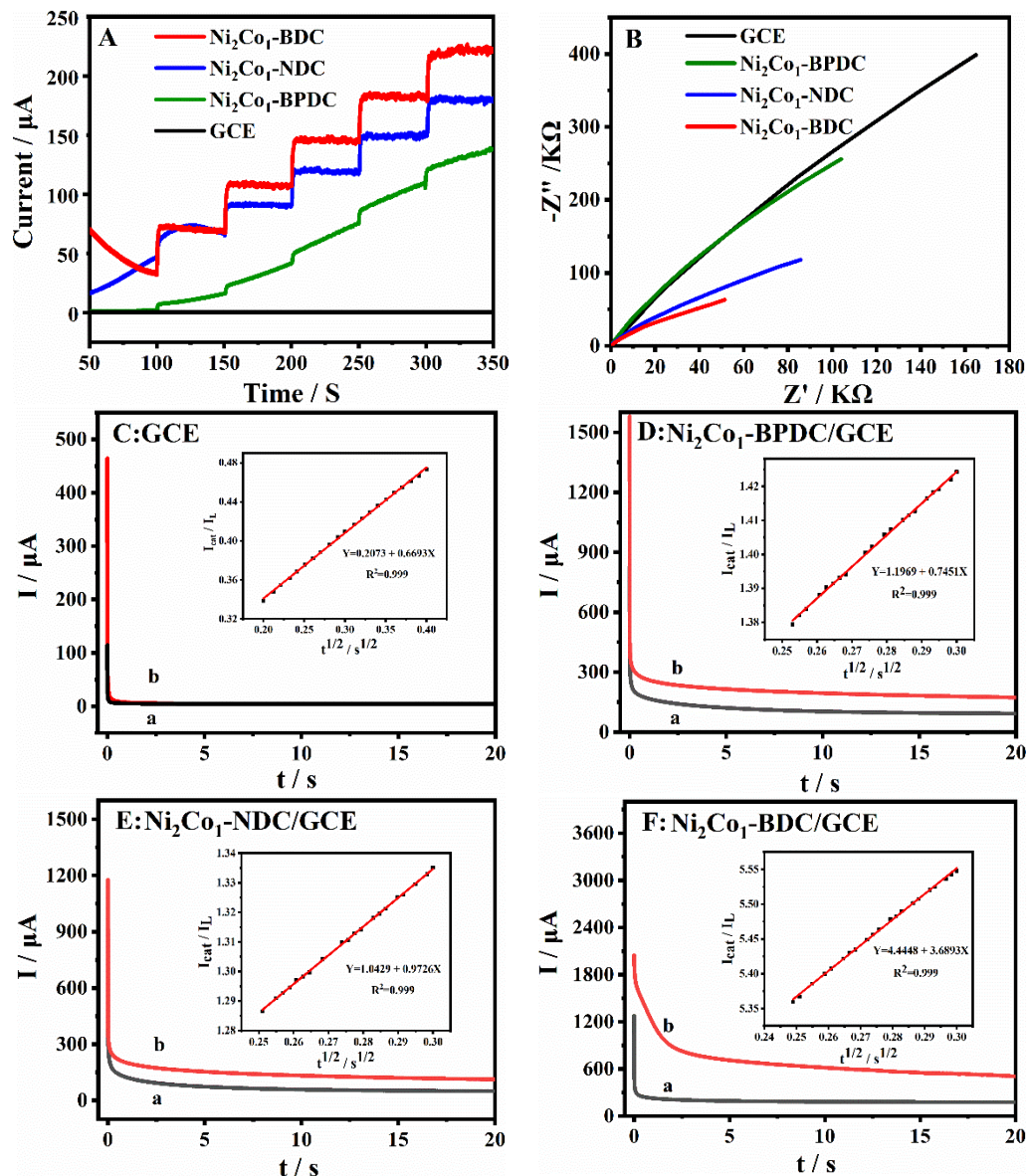


Figure 5. (A) i - t curves of different GCEs at the continuous injection of 0.1 mM glucose. (B) Nyquist curves of different GCEs in 0.1 M NaOH containing 0.1 mM glucose. Frequency range: 0.1 Hz–100 kHz. (C–F) Chronoamperometry behaviors on different GCEs in the absence (a) or presence of 1 mM glucose in 0.1 M NaOH (b), inset: plots of $I_{cat}/I_L-t^{1/2}$.

To explore the reason for the signal enhancement effects for the oxidation of glucose, electrochemical impedance spectroscopy (EIS) measurements were employed to investigate the electron transfer resistance of different Ni₂Co₁-L/GCEs during glucose oxidation. In the Nyquist plot, the semi-circle diameter represents the charge transfer resistance (R_{ct}) for the electrode surface active species [43]. Herein, based on Figure 5B, the fitted values of R_{ct} for the oxidation of glucose on the GCE, Ni₂Co₁-BPDC/GCE, Ni₂Co₁-NDC/GCE, and Ni₂Co₁-BDC/GCE were 85.4, 43.3, 27.2, and 12.0 K Ω , respectively. The greatly decreased R_{ct} values revealed that the Ni₂Co₁-BDC/GCE improved the electron transfer ability of glucose, consequently resulting in higher oxidation signals.

Subsequently, the chronoamperometry experiment was applied to study the electrochemical kinetics property, which can explain the signal enhancement mechanism more deeply. Figure 5C–F shows the charge (Q)-time (t) curves for the GCE, Ni₂Co₁-BPDC/GCE, Ni₂Co₁-NDC/GCE, and Ni₂Co₁-BDC/GCE in 0.1 M NaOH in the absence (a) and presence of 1 mM glucose (b). The apparent catalytic rate constant (K_{cat}) was determined according to the equation [44].

$$I_{cat}/I_L = (\pi k_{cat} C t)^{1/2} \quad (5)$$

where I_{cat} represents the catalytic current of analytes on the Ni₂Co₁-L/GCEs; I_L is the limiting current in the absence of analytes; C and t represent the analyte's concentration and time elapse, respectively. The linear regression equation between I_{cat}/I_L with $t^{1/2}$ is given in the inset of Figure 5C–F. The k_{cat} for the GCE, Ni₂Co₁-BPDC/GCE, Ni₂Co₁-NDC/GCE, and Ni₂Co₁-BDC/GCE was calculated as 1.43×10^2 , 1.77×10^2 , 3.01×10^2 , and $3.69 \times 10^3 \text{ M}^{-1}\cdot\text{s}^{-1}$. In summary, the Ni₂Co₁-BDC/GCE had the strongest electron transfer capacity and the highest electrocatalytic rate constant for glucose oxidation and consequently exhibited the largest signal response. The possible reasons are summarized as follows: First, the Ni, Co bimetallic provided active metal oxidation sites for glucose. Second, the 2D lamellar structure was more beneficial to the contact of active sites and accelerated electron transfer and mass transfer. In summary, the Ni₂Co₁-BDC/GCE had good electrochemical properties, which can be applied to the construction of a glucose electrochemical sensing platform.

To further investigate the reaction kinetic characteristics of the Ni₂Co₁-BDC/GCE for glucose oxidation, the CV curves of the electrode at different sweep rates (50–300 mV/s) were tested in the NaOH solution containing 0.1 mM glucose (Figure 6A). It can be seen from Figure 6B that both anodic and cathodic peak currents (I_p) increased in proportion to the square root of the scan rates. These results indicated that the electrochemical kinetics were diffusion-controlled. Moreover, the anodic peak potentials (E_{pa}) shifted more positively and the cathodic potentials (E_{pc}) shifted more negatively with increases in scan rates, which suggested the quasi-reversible electrochemical reaction process of the Ni₂Co₁-BDC on the electrode surface in the majority of activation sites [45]. Figure 6C presents the CVs of the Ni₂Co₁-BDC/GCE, including various concentrations of glucose. It was found that the peak current density of anodic oxidation increased with the augment of glucose concentration from 0 to 2 mM, which indicated that the Ni₂Co₁-BDC/GCE had good catalytic performance for glucose oxidation.

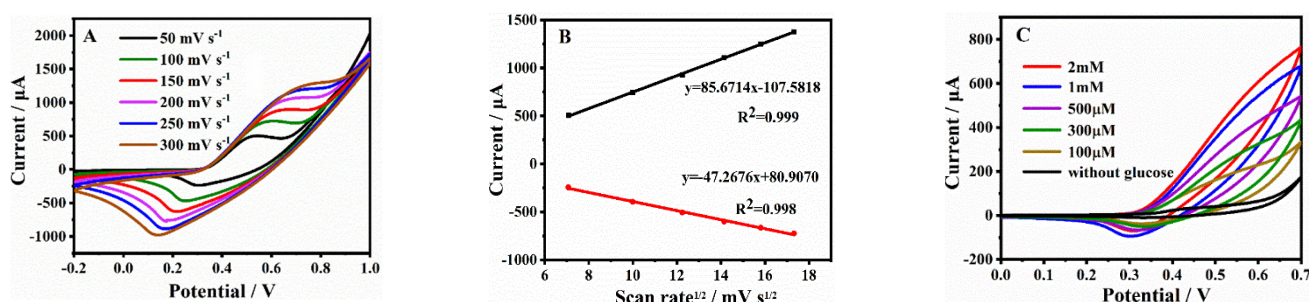


Figure 6. (A) CV curves of the Ni₂Co₁-BDC/GCE in the presence of 0.1 mM glucose at different scan rates from 50 to 300 mV/s in 0.1 M NaOH. (B) The plots of peak cathode and anode currents versus the square root of the scan rate. (C) CV curves of the Ni₂Co₁-BDC/GCE in 0.1 M NaOH in response to different glucose concentrations.

2.4. Non-Enzymatic Glucose Sensing Based on the Ni₂Co₁-BDC/GCE

The Ni₂Co₁-BDC/GCE was used to construct the enzyme-free glucose sensing because of its excellent electrochemical properties. To achieve the optimum sensing performance, the material preparation conditions, such as the effects of the bimetallic type and ratio (Ni, Ni:Co = 1:1, 2:1, 1:2, Co), the type and concentration of the applied base source (NaOH,

KOH, TEA, TEAH) on the glucose oxidation signal were optimized. As shown in Figure S2A–C, the strongest current step signal was obtained with the Ni₂Co₁-BDC/GCE (3 mmol KOH). Then, the test conditions (potential, modification amount, dispersing solvent) were also optimized. As shown in Figures 7A and S2D–F, the strongest current step signal was obtained under the test conditions of the test voltage of 0.50 V, dispersing solvent of DMF, and modification amount of 4 μ L (5 μ L Nafion).

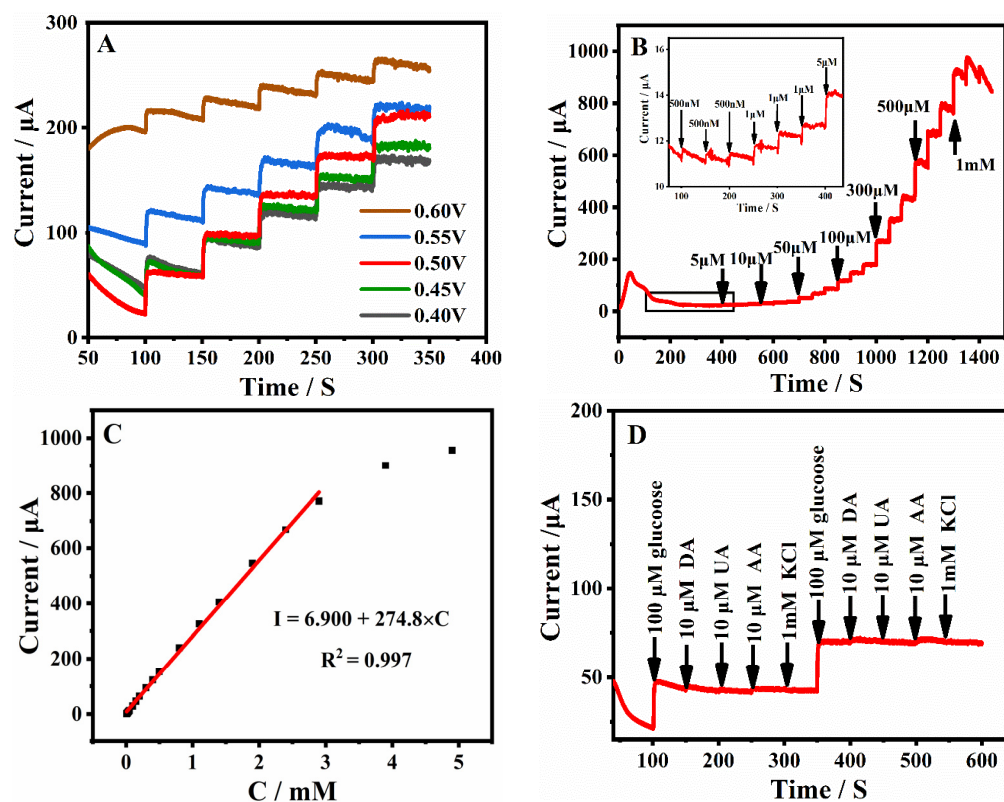


Figure 7. (A) *i-t* curves of Ni₂Co₁-BDC at different successive injections of 0.1 mM glucose. (B) Amperometric response of Ni₂Co₁-BDC to different concentrations of glucose at 0.50 V. (C) Linear function of amperometric response and glucose concentration. (D) Amperometric response of injected glucose (0.1 mM) and a series of interfering compounds at 0.50 V.

The relationship between glucose concentration and its oxidation signal was investigated under optimal conditions. Figure 7B shows the amperometric responses obtained for the Ni₂Co₁-BDC/GCE with successive additions of different concentrations of glucose in 0.1 M NaOH solution under the above optimal conditions. An excellent linear relationship was observed between the glucose concentration and its response signal in the range of 0.5 to 2899.5 μ M (Figure 7C). The linear regression equation was described as $I_{pa} (\mu A) = 274.8 C (mM) + 6.900$ with $R^2 = 0.997$. The sensitivity of the Ni₂Co₁-BDC/GCE was 3925.3 $\mu A mM^{-1} cm^{-2}$, and the detection limit was 0.29 μM ($S/N = 3$). The current response was gradually saturated with the gradual increase in glucose concentration, probably because the electrode surface was partially covered by adsorbed reaction intermediates, thus not providing enough electroactive sites for the oxidation process of glucose [46]. The Ni₂Co₁-BDC/GCE constructed in this study had a higher sensitivity, a lower detection limit, and a wider linearity range than the other transition metal electrochemical sensors constructed with enzyme-free glucose previously reported in the literature, as summarized in Table 1. Therefore, the Ni₂Co₁-BDC/GCE was found to have broad application prospects in the construction of glucose sensors.

The interference of some possible co-existing biomolecules with the detection of glucose signals at Ni₂Co₁-BDC/GCE electrodes was investigated. The concentration of

glucose in human serum is considered to be about 10 times higher than the concentration of the interfering biomolecule in the anti-interference test [47]. Therefore, the anti-interference test of the Ni₂Co₁-BDC/GCE was performed by successive addition of 100 μM glucose, 10 μM ascorbic acid (AA), 10 μM dopamine (DA), 10 μM uric acid (UA), and 1 mM KCl in 0.1 M NaOH. As can be seen from Figure 7D, the Ni₂Co₁-BDC/GCE had a very obvious current response to glucose, but the current response to these interferences was almost negligible, indicating that the sensor had good anti-interference ability.

Table 1. Performance comparison with previously reported glucose sensors.

Modified Electrode	Linear Range (μM)	LOD (μM)	Sensitivity (μA mM ⁻¹ cm ⁻²)	Ref.
Ni/ZAC-O NTAs	0–2800	1.02	1553	[48]
NiCo-hmf	1000–10,000	0.31	1739.04	[49]
NiO nanofiber/GO	2–600	0.8	1100	[50]
Mn ₃ O ₄ /N-doped rGO	2.5–529.5	1	1423.9	[51]
Ni@Cu-MOF	5–2500	1.67	1703.33	[52]
Ni ₂ Co ₁ -BDC/GCE	0.5–2899.5	0.29	3925.3	This work

Ni/ZAC-O NTAs: Ni-decorated ZrAlCo-O nanotube arrays; hmf: hydroxide microflowers.

Moreover, the reproducibility of the proposed Ni₂Co₁-BDC/GCE-based sensors was further evaluated. The relative standard deviation (RSD) of five independently manufactured Ni₂Co₁-BDC/GCE measurements of 100 μM glucose was calculated as 3.06%. Meanwhile, the RSD of five consecutive glucose additions with one Ni₂Co₁-BDC/GCE was only 2.14%. The lower RSD values justified the good reproducibility of the fabricated sensors. Several Ni₂Co₁-BDC/GCEs were stored in air at room temperature, and the current responses for 100 μM glucose were measured each day. The current response retained 93.37% of its original value after a week, as illustrated in Figure S2G, indicating good stability of the as-prepared electrochemical sensor.

To study the practical value of the Ni₂Co₁-BDC/GCE, the *i-t* method was used to detect human serum samples, and the accuracy and reliability of the electrode were evaluated. The standard glucose solution and different amounts of serum were added sequentially to 10 mL of 0.1 M NaOH at a voltage of 0.50 V (Figure S2H, Supporting Information). Then, blood glucose data measured from different human serum samples were compared with hospital tests, which showed satisfying results (Table 2). It can be seen that the blood glucose concentrations obtained from the Ni₂Co₁-BDC/GCE were well consistent with the hospital test results, which demonstrated the reliable practical value of the developed glucose sensor.

Table 2. Detection of glucose in human serum samples by the Ni₂Co₁-BDC/GCE and glucometer.

No.	by Glucometer (mM)	Ni ₂ Co ₁ -BDC/GCE (mM)	Relative Error
1	5.61	5.70	1.6%
2	6.04	6.05	0.2%
3	5.76	5.56	−3.5%
4	4.95	4.92	−0.61%

3. Materials and Methods

3.1. Reagents and Solutions

Co(CH₃COO)₂·4H₂O, Ni(CH₃COO)₂·4H₂O, 4,4'-biphenyldicarboxylic acid (H₂BPDC), 2,6-naphthalenedicarboxylic acid (H₂NDC), 1,4-benzenedicarboxylic acid (H₂BDC), KOH, NaOH, KCl, ascorbic acid (AA), uric acid (UA), dopamine (DA), glucose, Ethanol, and N,N-Dimethylformamide (DMF) were bought from Sinopharm Chemical Reagent (Shanghai, China). Pure water (15 MΩ) used in the experiments was supplied by a Millipore

System (Milli Q). Human serum was provided by the Second Affiliated Hospital of Hubei University of Science and Technology.

3.2. Instruments

Electrochemical performance experiments were carried out using a CHI 660E electrochemical workstation with a traditional three-electrode system. The saturated calomel electrode (SCE, Rosemead, CA, USA, in saturated KCl solution), platinum wire electrode, and the modified glassy carbon electrode (GCE) served as the reference electrode, counter electrode and the working electrode, respectively. The morphological characterization of the Ni₂Co₁-L MOFs was performed with a scanning electron microscope (SEM, Hitachi SU-8000) operated at an accelerating voltage of 10 kV. The composition and crystal structure of the Ni₂Co₁-L MOFs were checked by X-ray diffraction (XRD, Rigaku RINT 2500×) with Cu-Kα radiation. The Fourier transform infrared (FTIR) spectra of the samples were collected using the Avatar 360 Nicolet instrument.

3.3. Synthesis of Ni₂Co₁-L MOFs

In a typical preparation procedure, 0.67 mmol (0.1667 g) Ni(CH₃COO)₂·4H₂O and 0.33 mmol (0.0822 g) Co(CH₃COO)₂·4H₂O (Ni:Co = 2:1) were dissolved in 5 mL of DMF to form solution A. Meanwhile, 5 mL of ultrapure water was used to dissolve 3 mmol (0.1680 g) of KOH, and then 1 mmol of organic ligand (L = H₂BPDC, 0.2423 g; H₂NDC, 0.2162 g; H₂BDC, 0.1663 g) was added. After the above solution was clear, 5 mL of DMF was added to form solution B. Solution A was poured into solution B and reacted for 1 h under rapid stirring conditions. Finally, the mixed solution was centrifuged at 6000 rpm for 10 min. The obtained precipitate was centrifuged and washed by DMF and ethanol (1:1) several times and dried at 60 °C. Finally, Ni₂Co₁-BPDC, Ni₂Co₁-NDC, and Ni₂Co₁-BDC MOFs were obtained.

3.4. Preparation of the Ni₂Co₁-L MOFs Modified GCE

For the modification, 5 mg/mL of the material suspension was prepared by ultrasonic dispersion of 2.5 mg of the Ni₂Co₁-L MOFs powder in 495 μL of DMF, followed by the addition of 5 μL of Nafion. Meanwhile, the surface of the GCE (diameter: 3.0 mm) was polished using 0.05 μm alumina slurry and then washed with ethanol and ultrapure water in an ultrasonic bath. After that, 4 μL of Ni₂Co₁-L dispersion was pipetted onto the surface of the GCE, which was dried with an infrared baking lamp. Then, the Ni₂Co₁-BPDC/GCE, Ni₂Co₁-NDC/GCE, Ni₂Co₁-BDC/GCE were obtained and used as the working electrodes.

4. Conclusions

In summary, a series of Ni/Co bimetallic MOFs (Ni₂Co₁-BPDC, Ni₂Co₁-NDC, Ni₂Co₁-BDC) were successfully prepared under simple room temperature conditions. The effects of metal centers and ligand types on the morphology and electrochemical sensing properties of the Ni₂Co₁-L MOFs were demonstrated by different characterization approaches. It was demonstrated that Ni₂Co₁-BDC had an ultrathin and a homogeneous disk-like structure with a large electrochemical active area, which can expose abundant active sites. Moreover, an excellent electrochemical sensing capability for glucose detection was demonstrated by the prepared electrochemical sensor, which obtained a wider linear range, a lower detection limit, and a more stable interference immunity. Last, satisfactory results were also found for the detection of human serum samples, and the utility and accuracy were further demonstrated.

Supplementary Materials: The following supporting information can be downloaded at: <https://www.mdpi.com/article/10.3390/molecules28155649/s1>, Figure S1: (A) XRD and (B) FTIR spectra of monometallic and bimetallic MOF; (C) thermal gravimetric analysis (TGA) curve of Ni₂Co₁-L MOFs. Figure S2. *i-t* curves of MOFs under different experimental conditions with the continuous injection of 0.1 mM glucose. (A) metal center and scale; (B) types of alkali; (C) amounts of KOH; (D) the volume of Nafion; (E) modified volume; (F) dispersing solvents; (G) stability of the Ni₂Co₁-BDC/GCE in 0.1 M NaOH solution containing 0.1 mM Glu; (H) amperometric response of the Ni₂Co₁-BDC/GCE at successive additions of 20 μM glucose, 20 μL serum, and 40 μL serum, followed by 20 μM glucose. Table S1. The element content of Ni₂Co₁-BDC.

Author Contributions: Conceptualization, L.J.; methodology, Q.W. and Q.J.; software, Q.W.; validation, Q.W. and Q.J.; formal analysis, Q.W.; investigation, L.J.; resources, L.J. and P.H.; data curation, L.J. and P.H.; writing—original draft preparation, L.J.; writing—review and editing P.H.; visualization, L.J.; supervision, L.J.; project administration, P.H.; funding acquisition, L.J. and P.H. All authors have read and agreed to the published version of the manuscript.

Funding: This work was supported by the National Natural Science Foundation of China (62001159), the Special Fund Projects of Hubei Key Laboratory of Radiation Chemistry and Functional Materials (2022ZX05, 2021ZX07), and the Research and Development Fund Project of Hubei University of Science and Technology (2023-25GP02).

Institutional Review Board Statement: Not applicable.

Informed Consent Statement: Not applicable.

Data Availability Statement: Data will be made available upon reasonable request.

Conflicts of Interest: The authors declare no conflict of interest.

Sample Availability: Samples of the compounds are available from the authors upon reasonable request.

References

1. Beckles, G.L.; Bullard, K.M.K.; Saydah, S.; Imperatore, G.; Loustalot, F.; Correa, A. Life course socioeconomic position, allostatic load, and incidence of Type 2 diabetes among African American Adults: The Jackson Heart Study, 2000-04 to 2012. *Ethnic. Dis.* **2019**, *29*, 39. [[CrossRef](#)] [[PubMed](#)]
2. Liu, Y.A.; Chen, Q.Q.; Li, Y.Q.; Bi, L.L.; He, Z.Y.; Shao, C.X.; Jin, L.B.; Peng, R.Y.; Zhang, X.X. Advances in FGFs for diabetes care applications. *Life Sci.* **2022**, *310*, 121015. [[CrossRef](#)] [[PubMed](#)]
3. Jiao, Y.F.; Li, J.; Xiang, J.Y.; Chen, Z.B. Tungsten disulfide nanosheets-based colorimetric assay for glucose sensing. *Spectrochim. Acta Part A* **2020**, *242*, 118706. [[CrossRef](#)] [[PubMed](#)]
4. Sawayama, J.; Okitsu, T.; Nakamata, A.; Takeuchi, S.; Kawahara, Y. Hydrogel glucose sensor with in vivo stable fluorescence intensity relying on antioxidant enzymes for continuous glucose monitoring. *iScience* **2020**, *23*, 101243. [[CrossRef](#)]
5. Yang, S.Y.; Wang, Y.H.; Sheng, Q.L. Heterostructural NiCo₂O₄ nanocomposites for nonenzymatic electrochemical glucose sensing. *Electroanalysis* **2022**, *34*, 835–843. [[CrossRef](#)]
6. Chen, C.; Ran, R.; Yang, Z.Y.; Lv, R.T.; Shen, W.C.; Kang, F.Y.; Huang, Z.H. An efficient flexible electrochemical glucose sensor based on carbon nanotubes/carbonized silk fabrics decorated with Pt microspheres. *Sens. Actuator B Chem.* **2018**, *256*, 63–70. [[CrossRef](#)]
7. Mao, W.W.; Cai, B.; Ye, Z.Z.; Huang, J.Y. A nanostructured p-NiO/n-Bi₄Ti₃O₁₂ heterojunction for direct GOx electrochemistry and high-sensitivity glucose sensing. *Sens. Actuator B Chem.* **2018**, *261*, 385–391. [[CrossRef](#)]
8. Song, Y.; Zhu, C.Z.; Li, H.; Du, D.; Lin, Y.H. A nonenzymatic electrochemical glucose sensor based on mesoporous Au/Pt nanodendrites. *RSC Adv.* **2015**, *5*, 82617–82622. [[CrossRef](#)]
9. Huang, B.B.; Wang, Y.; Lu, Z.W.; Ye, J.S.; Du, H.J. One pot synthesis of palladium-cobalt nanoparticles over carbon nanotubes as a sensitive non-enzymatic sensor for glucose and hydrogen peroxide detection. *Sens. Actuator B Chem.* **2017**, *252*, 1016–1025. [[CrossRef](#)]
10. Niu, X.H.; Lan, M.B.; Chen, C.; Zhao, H.L. Nonenzymatic electrochemical glucose sensor based on novel Pt-Pd nanoflakes. *Talanta* **2012**, *99*, 1062–1067. [[CrossRef](#)]
11. Muqaddas, S.; Aslam, H.; Hassan, S.U.; Ashraf, A.R.; Asghar, M.A.; Ahmad, M.; Nazir, A.; Shoukat, R.; Kaleli, M.; Ibrahim, S.M.; et al. Electrochemical sensing of glucose and ascorbic acid via POM-based CNTs fiber electrode. *Mater. Sci. Eng. B-Adv.* **2023**, *293*, 116446. [[CrossRef](#)]
12. Chou, J.C.; Lin, S.H.; Lai, T.Y.; Kuo, P.Y.; Lai, C.H.; Nien, Y.H.; Su, T.Y. A facile fabrication of a potentiometric arrayed glucose biosensor based on nafion-GOX/GO/AZO. *Sensors* **2020**, *20*, 964. [[CrossRef](#)]
13. Juang, F.R.; Wang, T.M. Synthesis of Self-Assembled CuO Sphere Structures and Their Glucose Sensing Characteristics. *J. Electrochem. Soc.* **2021**, *168*, 037508. [[CrossRef](#)]

14. Guo, S.X.; Zhang, C.H.; Yang, M.; Wang, L.; Li, R.Q.; Ma, N. Three-dimensional flexible polyurethane decorated with Ni and reduced graphene oxide for high-sensitive sensing of glucose. *Mater. Chem. Phys.* **2022**, *278*, 125679. [[CrossRef](#)]
15. Xiong, C.; Tian, L.; Xiao, C.C.; Xue, Z.G.; Zhou, F.Y.; Zhou, H.; Zhao, Y.F.; Chen, M.; Wang, Q.P.; Qu, Y.T.; et al. Construction of highly accessible single Co site catalyst for glucose detection. *Sci. Bull.* **2020**, *65*, 2100–2106. [[CrossRef](#)] [[PubMed](#)]
16. Dai, X.L.; Deng, W.Q.; You, C.; Shen, Z.; Xiong, X.L.; Sun, X.P. A Ni₃N-Co₃N hybrid nanowire array electrode for high-performance nonenzymatic glucose detection. *Anal. Methods* **2018**, *10*, 1680–1684. [[CrossRef](#)]
17. Chen, T.; Liu, D.N.; Lu, W.B.; Wang, K.Y.; Du, G.; Asiri, A.M.; Sun, X.P. Three-dimensional Ni₂P nanoarray: An efficient catalyst electrode for sensitive and selective nonenzymatic glucose sensing with high specificity. *Anal. Chem.* **2016**, *88*, 7885–7889. [[CrossRef](#)]
18. Wang, F.; Zhao, D.S.; Li, W.Q.; Zhang, H.H.; Li, B.; Hu, T.P.; Fan, L.M. Rod-shaped unitsbased cobalt (II) organic framework as an efficient electrochemical sensor for uric acid detection in serum. *Microchem. J.* **2023**, *185*, 108154. [[CrossRef](#)]
19. Ma, L.; Svec, F.; Lv, Y.Q.; Tan, T.W. Engineering of the filler/polymer interface in metal-organic framework-based mixed-matrix membranes to enhance gas separation. *Chem-Asian J.* **2019**, *14*, 3502–3514. [[CrossRef](#)] [[PubMed](#)]
20. Mullangi, D.; Evans, H.A.; Yildirim, T.; Wang, Y.X.; Deng, Z.Y.; Zhang, Z.Q.; Mai, T.T.; Wei, F.X.; Wang, J.; Walker, A.R.H.; et al. Noncryogenic Air Separation Using Aluminum Formate Al(HCOO)₃ (ALF). *J. Am. Chem. Soc.* **2023**, *145*, 9850–9856. [[CrossRef](#)]
21. Xiao, P.T.; Xu, Y.X. Recent progress in two-dimensional polymers for energy storage and conversion: Design, synthesis, and applications. *J. Mater. Chem. A* **2018**, *6*, 21676–21695. [[CrossRef](#)]
22. Souri, Z.; Mazloum-Ardakani, M.; Alizadeh, S.; Nematollahi, D. Template-free electrodeposition of sponge-like porous polymer interwoven with the bimetallic metal-organic framework and reduced graphene oxide and application in energy storage device. *J. Energy Storage* **2022**, *55*, 105381. [[CrossRef](#)]
23. Zhang, Z.Q.; Deng, Z.Y.; Evans, H.A.; Mullangi, D.; Kang, C.J.; Peh, S.B.; Wang, Y.X.; Brown, C.M.; Wang, J.; Canepa, P.; et al. Exclusive Recognition of CO₂ from Hydrocarbons by Aluminum Formate with Hydrogen-Confined Pore Cavities. *J. Am. Chem. Soc.* **2023**, *145*, 11643–11649. [[CrossRef](#)] [[PubMed](#)]
24. Li, W.Q.; Zhao, D.S.; Li, W.C.; Wen, R.M.; Liu, X.; Liu, L.Y.; Li, T.; Fan, L.M. Chemorobust dye-encapsulated framework as dual-emission self-calibrating ratiometric sensor for intelligent detection of toluene exposure biomarker in urine. *Spectrochim. Acta Part A* **2023**, *296*, 122637. [[CrossRef](#)]
25. Zhao, K.M.; Zhu, W.W.; Liu, S.Q.; Wei, X.L.; Ye, G.Y.; Su, Y.K.; He, Z. Two-dimensional metal-organic frameworks and their derivatives for electrochemical energy storage and electrocatalysis. *Nanoscale Adv.* **2020**, *2*, 536–562. [[CrossRef](#)] [[PubMed](#)]
26. Zhao, D.S.; Li, W.Q.; Wen, R.M.; Li, W.C.; Liu, X.; Zhang, X.T.; Fan, L.M. Tb (III) functionalized MOF based self-calibrating sensor integrated with logic gate operation for efficient epinephrine detection in serum. *J. Rare Earths* **2023**. [[CrossRef](#)]
27. Han, Y.; Liu, Z.J.; Zheng, F.F.; Bai, Y.X.; Zhang, Z.Q.; Li, X.G.; Xiong, W.W.; Zhang, J.H.; Yuan, A.H. Two-dimensional flower-like cobalt-porphyrin MOF/rGO composite anodes for high-performance Li-ion batteries. *J. Alloys. Compd.* **2021**, *881*, 160531. [[CrossRef](#)]
28. Ji, L.D.; Wang, Q.; Peng, L.H.; Li, X.Y.; Zhu, X.M.; Hu, P. Cu-TCPP Nanosheets-Sensitized Electrode for Simultaneous Determination of Hydroquinone and Catechol. *Materials* **2022**, *15*, 4625. [[CrossRef](#)]
29. Han, L.J.; Zheng, D.; Zheng, H.G.; Ma, J.; Chen, S.G. A Highly Solvent-Stable Metal-Organic Framework Nanosheet: Morphology Control, Exfoliation, and Luminescent Property. *Small* **2018**, *14*, 1703873. [[CrossRef](#)]
30. Chen, L.Y.; Wang, H.F.; Li, C.X.; Xu, Q. Bimetallic metal-organic frameworks and their derivatives. *Chem. Sci.* **2020**, *11*, 5369–5403. [[CrossRef](#)]
31. Niu, S.Y.; Li, C.H.; Huo, J.; Dong, W.R.; Hankari, S.E.; Liang, Y.; Li, Q.L. Ultrathin Trimetal-Organic Framework Nanosheet Electrocatalysts for the Highly Efficient Oxygen Evolution Reaction. *ACS Omega* **2021**, *6*, 13946–13952. [[CrossRef](#)] [[PubMed](#)]
32. Mullangi, D.; Dhavale, V.; Shalini, S.; Nandi, S.; Collins, S.; Woo, T.; Kurungot, S.; Vaidhyanathan, R. Low-Overpotential Electrocatalytic Water Splitting with Noble-Metal-Free Nanoparticles Supported in a sp³ N-Rich Flexible COF. *Adv. Energy Mater.* **2016**, *6*, 1600110. [[CrossRef](#)]
33. Nandi, S.; Singh, S.K.; Mullangi, D.; Illathvalappil, R.; George, L.; Vinod, C.P.; Kurungot, S.; Vaidhyanathan, R. Low band gap benzimidazole COF supported Ni₃N as highly active OER catalyst. *Adv. Energy Mater.* **2016**, *6*, 1601189. [[CrossRef](#)]
34. Pan, L.; Ching, N.; Huang, X.Y.; Li, J. Reactions and Reactivity of Co-bpdc Coordination Polymers (bpdc = 4,4'-biphenyldicarboxylate). *Inorg. Chem.* **2000**, *39*, 5333–5340. [[CrossRef](#)]
35. Carton, A.; Mesbah, A.; Mazet, T.; Porcher, F.; François, M. Ab initio crystal structure of nickel (II) hydroxy-terephthalate by synchrotron powder diffraction and magnetic study. *Solid State Sci.* **2007**, *9*, 465–471. [[CrossRef](#)]
36. Du, Y.; Thompson, A.L.; O'Hare, D. Resin-assisted solvothermal synthesis of metal-organic frameworks. *Chem. Commun.* **2008**, *45*, 5987–5989. [[CrossRef](#)]
37. Inoue, S.; Fujihara, S. Liquid-Liquid biphasic synthesis of layered zinc hydroxides intercalated with long-chain carboxylate ions and their conversion into ZnO nanostructures. *Inorg. Chem.* **2011**, *50*, 3605–3612. [[CrossRef](#)]
38. Rawool, C.R.; Karna, S.P.; Srivastava, A.K. Enhancing the supercapacitive performance of Nickel based metal organic framework-carbon nanofibers composite by changing the ligands. *Electrochimica. Acta* **2019**, *294*, 345–356. [[CrossRef](#)]
39. Ahsan, M.A.; Jabbari, V.; Imam, M.A.; Castro, E.; Kim, H.; Curry, M.L.; Valles-Rosales, D.J.; Noveron, J.C. Nanoscale nickel metal organic framework decorated over graphene oxide and carbon nanotubes for water remediation. *Sci. Total Environ.* **2020**, *698*, 134214. [[CrossRef](#)]

40. Cavka, J.H.; Jakobsen, S.; Olsbye, U.; Guillou, N.; Lamberti, C.; Bordiga, S.; Lillerud, K.P. A new zirconium inorganic building brick forming metal organic frameworks with exceptional stability. *J. Am. Chem. Soc.* **2008**, *130*, 13850–13851. [[CrossRef](#)]
41. Ji, L.D.; Li, F.; Li, C.L.; Hu, P. Solvent-exfoliated Cu-TCPP nanosheets: Electrochemistry and sensing application in simultaneous determination of 4-aminophenol and acetaminophen. *Microchem J.* **2022**, *181*, 107688. [[CrossRef](#)]
42. Gumilar, G.; Kaneti, Y.V.; Henzie, J.; Chatterjee, S.; Na, J.; Yulianto, B.; Nugraha, N.; Patah, A.; Bhaumik, A.; Yamauchi, Y. General synthesis of hierarchical sheet/plate-like M-BDC (M= Cu, Mn, Ni, and Zr) metal-organic frameworks for electrochemical non-enzymatic glucose sensing. *Chem. Sci.* **2020**, *11*, 3644–3655. [[CrossRef](#)] [[PubMed](#)]
43. Katz, E.; Willner, I. Probing biomolecular interactions at conductive and semiconductive surfaces by impedance spectroscopy: Routes to impedimetric immunosensors, DNA-sensors, and enzyme biosensors. *Electroanalysis* **2003**, *15*, 913–947. [[CrossRef](#)]
44. Dong, Y.Y.; Zhou, M.; Zhang, L. 3D multiporous Co, N co-doped MoO₂/MoC nanorods hybrids as improved electrode materials for highly sensitive simultaneous determination of acetaminophen and 4-aminophenol. *Electrochim. Acta* **2019**, *302*, 56–64. [[CrossRef](#)]
45. Rezaeinasab, M.; Benvidi, A.; Tezerjani, M.D.; Jahanbani, S.; Kianfar, A.H.; Sedighipoor, M. An electrochemical sensor based on Ni (II) complex and multi wall carbon nano tubes platform for determination of glucose in real samples. *Electroanalysis* **2017**, *29*, 423–432. [[CrossRef](#)]
46. Wu, G.H.; Song, X.H.; Wu, Y.F.; Chen, X.M.; Luo, F.; Chen, X. Non-enzymatic electrochemical glucose sensor based on platinum nanoflowers supported on graphene oxide. *Talanta* **2013**, *105*, 379–385. [[CrossRef](#)]
47. Wei, Z.Y.; Zhu, W.X.; Li, Y.; Ma, Y.Y.; Wang, J.; Hu, N.; Suo, Y.R.; Wang, J.L. Conductive leaflike cobalt metal-organic framework nanoarray on carbon cloth as a flexible and versatile anode toward both electrocatalytic glucose and water oxidation. *Inorg. Chem.* **2018**, *57*, 8422–8428. [[CrossRef](#)]
48. Wu, X.; Chen, F.; Huang, M.; Dan, Z.; Qin, F. Ni-decorated ZrAlCo-O nanotube arrays with ultrahigh sensitivity for non-enzymatic glucose sensing. *Electrochim. Acta* **2019**, *311*, 201–210. [[CrossRef](#)]
49. He, L.; Cao, J.; Li, J.W.; Li, X.; Fan, P.P.; Yang, Y. Highly efficient non-enzymatic glucose biosensor based on Ni_{0.5}Co_{0.5}(OH)₂ microflowers adorned glassy carbon electrode. *Mater. Lett.* **2021**, *301*, 130197. [[CrossRef](#)]
50. Zhang, Y.Q.; Wang, Y.Z.; Jia, J.B.; Wang, J.G. Nonenzymatic glucose sensor based on graphene oxide and electrospun NiO nanofibers. *Sens. Actuator B-Chem.* **2012**, *171*, 580–587. [[CrossRef](#)]
51. Yang, S.L.; Li, G.; Wang, G.F.; Zhao, J.H.; Gao, X.H.; Qu, L.B. Synthesis of Mn₃O₄ nanoparticles/nitrogen-doped graphene hybrid composite for nonenzymatic glucose sensor. *Sens. Actuator B-Chem.* **2015**, *221*, 172–178. [[CrossRef](#)]
52. Xue, Z.; Jia, L.; Zhu, R.R.; Du, L.; Zhao, Q.H. High-performance non-enzymatic glucose electrochemical sensor constructed by transition nickel modified Ni@ Cu-MOF. *J. Electroanal. Chem.* **2020**, *858*, 113783. [[CrossRef](#)]

Disclaimer/Publisher's Note: The statements, opinions and data contained in all publications are solely those of the individual author(s) and contributor(s) and not of MDPI and/or the editor(s). MDPI and/or the editor(s) disclaim responsibility for any injury to people or property resulting from any ideas, methods, instructions or products referred to in the content.